J Mar Sci Technol (2005) 10:131–146
DOI 10.1007/s00773-004-0189-3

Journal of
Marine Science
and Technology


# Steady sailing performance of a hybrid-sail assisted bulk carrier

Toshifumi Fujiwara[1], Grant E. Hearn[2], Fumitoshi Kitamura[1], Michio Ueno[1], and Yoshimasa Minami[1]

[1] National Maritime Research Institute (NMRI), 6-38-1 Shinkawa, Mitaka, Tokyo 181-0004, Japan
[2] School of Engineering Sciences, University of Southampton, Highfield, Southampton, UK

**Abstract** The steady sailing performance of a sail-assisted bulk carrier is investigated utilising towing-tank derived hydrodynamic derivatives and wind tunnel measured aerodynamic properties of the sails and the ship. The aerodynamic characteristics investigated include the ship hull at the fully-loaded draught, the sail–sail interaction effects for two sets of four identical hybrid-sails, and the sail–hull interaction effects for the same two sets of identical sails in the presence of the selected bulk carrier hull-form. This is in addition to lift–drag measurements of single isolated sails of each shape. The form of the two sets of soft sails was rectangular and triangular. This paper is concerned with assessing the benefits of a sail-assisted ship operation, and hence a steady-state rather than complete time-domain integrations of the governing equations are reported. The results of the completed analysis suggest that the benefits of the derived sail generated driving force are greater than the overhead of equipping the ship with a selected system of hybrid-sails. Sail-assisted ships could represent an important contribution to an improving global environment by reducing the demands for a driving force through the propeller.

**Key words** Global warming control · Sail–sail and sail–hull form interaction · Sail-assisted ship · Steady-sailing performance · Economic benefit

**List of symbols**

| | |
|---|---|
| $a_H$ | Kijima et al.[1] rudder force coefficient |
| $A_L$, $A_T$ | Lateral and transverse projected area of ship excluding projected area of sails (m²) |
| $A_R$ | Rudder area (m²) |
| $B$ | Breadth of ship (beam) (m) |
| BHP | Brake horsepower (ps), with 1 ps = 735.49875 W and ps denoting the German unit of Pferdestärke (www.sciencedaily.com/encyclopedia/horsepower) |
| $C_B$ | Block coefficient of ship |
| $C_D$, $C_L$ | Drag and lift force coefficients of sails |
| $C_{PA}$, $C_{WA}$ | Prismatic and water plane area coefficients |
| $C_X$, $C_Y$, $C_N$, $C_K$ | Wind force and moment coefficients |
| $d$ | Ship draught in fully-loaded condition (m) |
| $d_{Air}$ | Air draught from the water surface to the top of the sail with ship in a fully-loaded condition (m) |
| $D$ | Ship depth (m) |
| DHP | Delivered horsepower (ps) |
| $D_P$ | Propeller diameter (m) |
| $e_A$, $e'_A$ | Geometric parameters defined in Eq. 6h |
| $f_A$ | Fujii and Tsuda's[2] normal force parameter for rudder |
| Fn | Froude number |
| FOC | Fuel oil consumption |
| $F'_N$ | Non-dimensional normal rudder force |
| $g$ | Gravitational acceleration (m/s²) |
| $G$ | Centre of gravity of ship |
| GM | Metacentric height measured from centre of gravity (m) |
| $h$ | Rudder height (m) |
| $I_{XX}$, $I_{ZZ}$ | Heel and yaw related mass moments of inertia |
| $J$ | Advance coefficient of propeller |
| $k$ | Propeller and rudder wake-related coefficient defined in Eq. 6e |
| $K$ | Heel moment of ship (Nm) |
| KG | Height of the center of gravity from the keel (m) |
| $K_S$ | Heel moment caused by sails (Nm) |
| $K_T(J)$, $K_Q(J)$ | Advance coefficient dependent propeller thrust and torque coefficients |
| $K'_A$, $K'_H$, $K'_R$ | Non-dimensional contribution to heel moment associated with wind, hull hydrodynamics, and rudder forces |
| $K'_\beta$, $K'_\phi$, ... | Hydrodynamic derivative associated with $K'_H$ moment model of Yoshimura et al.[3] |
| $L_{PP}$, $L_{OA}$ | Ship length between perpendiculars and the overall length of ship (m) |
| $m$, $m_{Sa}$ | Ship and sail mass (kg) |
| MCR | Maximum continuous rating of diesel engine (ps) |

*Address correspondence to:* T. Fujiwara (fujiwara@nmri.go.jp)
Received: July 7, 2004 / Accepted: November 22, 2004

| | |
|---|---|
| $n$ | Propeller revolution (rps) |
| $N$ | Yaw moment (Nm) |
| $N_A$ | Number of true wind directions used in statistical analyses |
| $N_P$ | Number of discrete ranges of wind speed used in the North Pacific Ocean database |
| $N_S$ | Yaw moment caused by sails (Nm) |
| $N'_A, N'_H, N'_R$ | Non-dimensional contribution to yaw moment associated with wind, hull hydrodynamics, and rudder forces |
| $N'_\beta, N'_\phi, \ldots$ | Hydrodynamic derivative associated with $N'_H$ moment model of Yoshimura et al.[3] |
| O | Origin of body axes |
| OG | Gravity height from water surface (m) (positive downwards) |
| $P$ | Propeller pitch (m) |
| $P_{U_T}$ | Probability distribution of true wind velocity $U_T$ |
| $r$ | Yaw angular velocity defined in Fig. 4 (rad/s) |
| $R_0, R_1, R_2, R_3$ | Coefficients of calm water resistance contribution to surge hydrodynamic force $X_H$ |
| $s$ | Propeller related coefficient defined in Eq. 6e |
| $S$ | Total sail area (m$^2$) |
| $t_P$ | Thrust reduction coefficient of propeller |
| $t_R$ | Kijima et al.[1] rudder thrust reduction coefficient |
| TB | Thrust benefit defined in Eq. 8 (%) |
| $u, v$ | Longitudinal and lateral ship velocities defined in Figs. 4 and 8 (m/s) |
| $u_x, u_y$ | Longitudinal and lateral apparent wind velocity components defined in Fig. 8 (m/s) |
| $U$ | Steady advance speed of ship (m/s) |
| $U_A$ | Apparent steady wind velocity defined in Fig. 8 (m/s) |
| $U_T$ | True wind speed defined in Figs. 4 and 8 (m/s) |
| $U'_R$ | Non-dimensional effective speed of water flow over rudder introduced in Eq. 6d |
| $w_P, w_{P0}, w_R, w_{R0}$ | Propeller wake and rudder related coefficients of Eqs. 5b, 5c, and 6e |
| $x, y, z$ | Cartesian coordinates |
| $x_R, z_R$ and $x'_R, z'_R$ | Dimensional (m) and non-dimensional coordinates of rudder reference point defined in text |
| $x'_H$ | Kijima et al.[1] rudder coefficient |
| $X, Y$ | Longitudinal and lateral forces (N) defined in Fig. 4 |
| $X_S, Y_S$ | Longitudinal and lateral forces caused by sails (N) |
| $X'_A, X'_H, X'_P, X'_R$ | Non-dimensional contribution to longitudinal force associated with wind, hull hydrodynamics, propeller and rudder forces |
| $X'_{\beta\beta}, X'_{\beta\phi}, \ldots$ | Hydrodynamic derivative associated with $X'_H$ force model of Yoshimura et al.[3] |
| $X'_0$ | Non-dimensional propeller thrust force |
| $Y'_A, Y'_H, Y'_R$ | Non-dimensional contribution to lateral force associated with wind, hull hydrodynamics, and rudder forces |
| $Y'_\beta, Y'_\phi, \ldots$ | Hydrodynamic derivative associated with $Y'_H$ force model of Yoshimura et al.[3] |
| $\alpha_R$ | Effective inflow rudder angle defined in Eq. 6f (°) |
| $\beta$ | Drift angle defined in Fig. 4 (°) |
| $\gamma$ | Boom angle of sail defined in Fig. 3 (°) |
| $\gamma_R$ | Effective rudder angle coefficient defined in Eq. 6g |
| $\delta$ | Actual rudder angle defined in Fig. 4 (positive to starboard) (°) |
| ΔBHP | Brake horsepower differential for a ship with and without sail systems (ps) |
| ΔFOC | Fuel oil consumption differential for a ship with and without sail systems |
| $\eta_P$ | Propeller diameter to rudder height ratio required in Eq. 6e |
| $\eta_{PC}, \eta_{QC}$ | Propulsive and quasi-propulsive coefficients |
| $\eta_0$ | Open water propeller efficiency presented in Fig. 7 |
| $\Lambda$ | Rudder aspect ratio defined as $h^2/A_R$ |
| $\zeta$ | Slat orientation angle defined in Fig. 3 (°) |
| $\pi$ | Mathematical constant |
| $\rho, \rho_A$ | Density of water and air, respectively (kg/m$^3$) |
| $\sigma_A$ | Form parameter of ship's after-part defined in Eq. 6e |
| $\phi$ | Ship heel angle defined in Fig. 4 (°) |
| $\psi$ | Ship heading angle relative to true wind defined in Figs. 4 and 8 (°) |
| $\psi'$ | Ship heading angle relative to apparent wind defined in Fig. 8 (°) |

## Introduction

The marine industry burns large amounts of fossil fuel that releases $CO_2$ into the atmosphere, and hence contributes to global warming. Whilst the environmental impact of global warming is of concern to mankind per se, it would be unrealistic for modern engine driven ships to completely revert to sail based propulsion. However, many ships must endure strong winds, as they perform the task of efficiently transporting large volumes of cargo of infinite variety around the world, and hence sail-assisted propulsion would represent the utilisation of this natural energy with little negative environmental impact. The economic viability and an assessment of the reduced engine generated thrust necessitates understanding the steady-state performance of a sail-assisted ship. Therefore, this paper undertakes the necessary calculations to allow such an assessment by exploiting a recently generated extended database of aerodynamic lift and drag characteristics for a modern design of hybrid-sail.

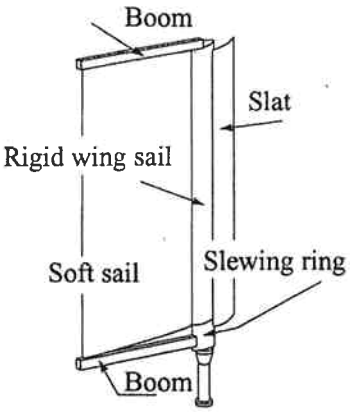


**Fig. 1.** Hybrid-sail consisting of slat, rigid wing sail and soft sail attached to booms

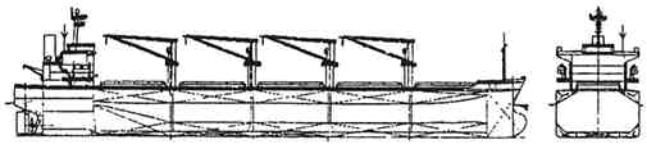

**Fig. 2.** Geometric form of the bulk carrier modelled

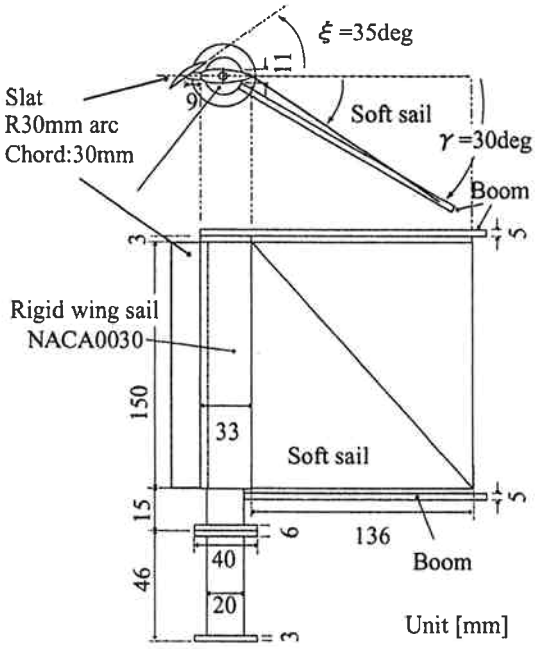


**Fig. 3.** Plan and side elevation of model scale hybrid-sail

**Table 1.** Principal ship particulars for the bulk carrier and scaled model

| | Full scale | Aero. model | Hydro. model |
|---|---|---|---|
| $L_{OA}$ (m) | 185 | 1.254 | — |
| $L_{PP}$ (m) | 177 | 1.200 | 2.980 |
| $B$ (m) | 30.4 | 0.206 | 0.538 |
| $D$ (m) | 16.5 | 0.112 | — |
| $d$ (m) | 11.6 | 0.079 | 0.180 |
| $d_{air}$ (m) | 38.0 | 0.258 | — |
| $A_T$ (m²) | 553 | 0.025 | — |
| $A_L$ (m²) | 1997 | 0.092 | — |
| GM (m) | 2.00 | — | — |
| KG (m) | 9.75 | — | — |
| $C_B$ | 0.80 | — | 0.80 |
| $C_{PA}$ | 0.75 | — | 0.75 |
| $C_{WA}$ | 0.77 | — | 0.77 |

In earlier wind tunnel based experimental studies, Fujiwara et al.[4,5] investigated the aerodynamic characteristics of single isolated hybrid-sails of different size and aspect ratio. The selected hybrid-sail consists of a slat, a rigid wing sail and a soft sail attached to a boom as illustrated in Fig. 1. The cited experimental measurements demonstrate that the driving force generated by such sails significantly exceeds the driving force of the earlier simpler sails of Ishihara et al.[6] and Matsumoto et al.[7] designed when fossil fuel prices first necessitated the operation of sail-assisted ships in the 1980s. The task of assessing the steady-state performance of a sail-assisted ocean-going bulk carrier was partially performed by Minami et al.[8,9] through the application of the isolated hybrid-sail results of Fujiwara et al.[4,5]

Completion of the steady-state sailing performance analysis of the bulk carrier presented in Fig. 2, to assess the benefits of sail-assisted ship operations in detail, requires improved aerodynamic characterisation of the sails to provide assessment and understanding of the effect of the sail–sail and sail–hull form interaction for a practical sail configuration. Fujiwara et al.[10] investigated these interaction effects for the bulk carrier hull form for 4 hybrid-sails with rectangular soft sails and then extended the study to compare hybrid-sails with rectangular and triangular soft sails in Fujiwara et al.[11] In each case the aspect ratio and the sail area indicated in Fig. 3 represent a compromise between the best rectangular and the best triangular sails identified in the earlier study,[4,5] the crane arrangements of Fig. 2, the ship dimensions of Table 1 and the air draught condition required to allow safe operation world-wide at the ballasted condition. The influence of the sail form on the steady-state sailing performance of the ocean-going bulk carrier is especially investigated in this paper.

Formulation of the steady-state equations is based on the ship manoeuvering simulation equations. The steady-state solutions are sought using the measured

aerodynamic details for isolated sails as well as the indicated interaction effects for both sets of hybrid-sail based on rectangular and triangular soft sails. Prior to closure of the paper, the benefits of the hybrid-sail are finally estimated in terms of reduced brake horse power (BHP) and reduced fuel oil consumption (FOC), using the optimum setting of the sails, for operations in the North Pacific Ocean.

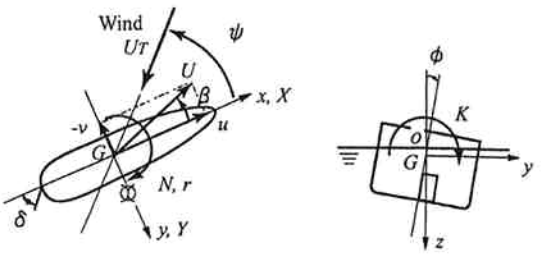


**Fig. 4.** Coordinate definitions and force/moment sign convention for ship hull loading and sailing condition

## Formulation and solution of steady sailing equations

In this section of the paper, the governing equations and the steady-state sailing conditions are presented with idealisations of the different hydrodynamic and aerodynamic loads the sail-assisted ship will experience. The governing equations of motion are modelled using the MMG formulation,[12] with the steady sailing conditions are selected in a manner consistent with the investigation of the sail training ship *Nippon-maru* by Yoshimura et al.[3] Hydrodynamic derivative coefficients for the selected bulk carrier have been determined experimentally using towing tank tests with a tanker model, with similar $L/B$, $B/d$ and an identical block coefficient, subjected to appropriate variations of drift angle, $\beta$, and heel angle, $\phi$, for the required cruising speed. As a new approach the rudder forces and moments are defined in terms of Kijima et al.[1] in the calculation of steady-state sailing. Calculations on the steady-state sailing conditions are undertaken for a ship in the fully-loaded condition. The determination of the extended aerodynamic sail data, with all the required interaction effects, is discussed in some detail elsewhere.[11]

### *Ship motion equations*

Ship manoeuvering equations are most commonly expressed in terms of the horizontal degrees of freedom of surge, sway and yaw. In the case of a sail-assisted ship, heeling will occur owing to the wind loading of the hybrid-sails installed, and therefore the roll degree of freedom must be addressed. The resulting roll motion is assumed to be more significant than the other vertical plane motions of pitch and heave, which are therefore ignored. Consequently, the equations assumed to govern the ship motions, consistent with the MMG model[12] and written with respect to the centre of gravity of the ship, have the general form

$$\begin{aligned} m\dot{u} - mvr &= X \\ m\dot{v} + mur &= Y \\ I_{ZZ}\dot{r} &= N \\ I_{XX}\ddot{\phi} &= K - GM \cdot g \cdot m \cdot \sin\phi \end{aligned} \tag{1}$$

The ship mass, the yaw and roll moments of inertia of the ship, with respect to the vertical $z$-axis and the horizontal $x$-axis, are denoted by $m$, $I_{ZZ}$, and $I_{XX}$, whereas the longitudinal, lateral, and yaw velocities with respect to the centre of gravity of the ship are designated $u$, $v$ and $r$. Furthermore, the external forces and moments designated $X$, $Y$, $N$ and $K$, defined in Fig. 4, have components arising from the hydrodynamic characteristics of the hull, the propeller generated thrust and torque, the rudder reactive loads and the wind forces acting on both the hull and the set of four hybrid-sails.

The assumed transverse metacentric height GM was established from well-tested empirical graphical relationships[13] (used by many shipbuilders in Japan) and the known ship geometric characteristics. Naturally the ship GM value is modified to take into account the weight of the added sails; the decrease in GM is of the order of 21 cm and 12 cm for the rectangular and triangular soft sail forms of the selected hybrid-sails, respectively. Steady sailing will persist when there are no rates of change in the ship motion parameters $u$, $v$, $r$ and $\phi$. Under the conditions of steady sailing, Eq. 1 reduces to the four mathematical conditions

$$\begin{aligned} &X = 0, \qquad Y = 0, \qquad N = 0 \\ &K - \mathrm{GM} \cdot g \cdot m \cdot \sin\phi = 0 \end{aligned} \tag{2}$$

These equations will be solved for the steady speed of advance of the ship, the drift angle, the resulting heel angle and the rudder setting, $U$, $\beta$, $\phi$ and $\delta$, respectively, for different true wind speeds, $U_T$, and the true wind direction, $\psi$. An interpretation of the solutions determined is addressed once the external force and moment details required for particularising Eq. 2 to the selected hull form and hybrid-sails have been presented.

## External loads experienced by a ship

Using the suffices H, P, R, A to indicate the contribution of the hull, propeller, rudder, and wind to the external forces and moments, and the superscripted

prime to indicate a non-dimensional quantity, one may write

$$X\Big/\frac{\rho}{2}L_{PP}dU^2 = X'_H + X'_P + X'_R + X'_A$$
$$Y\Big/\frac{\rho}{2}L_{PP}dU^2 = Y'_H + Y'_R + Y'_A$$
$$N\Big/\frac{\rho}{2}L_{PP}{}^2dU^2 = N'_H + N'_R + N'_A$$
$$K\Big/\frac{\rho}{2}L_{PP}d^2U^2 = K'_H + K'_R + K'_A \quad (3)$$

The different length scales used here are the length between the perpendiculars, $L_{PP}$, and the ship draught for the fully-loaded condition, $d$.

*Hull hydrodynamic loads*

In the case of zero drift angle and zero heel angle the only hydrodynamic force to overcome is the calm water resistance, since wave influences are not to be addressed. To take into account the influences of the drift and heel angles the resulting forces and moments are expressed in the hydrodynamic derivative form suggested by Yoshimura et al.[3] in their analysis of the sail training ship *Nippon-maru*. Hence, the hull hydrodynamic loads are expressed in the form

$$X'_H = X'_0 + X'_{\beta\beta}\beta^2 + X'_{\beta\phi}\beta\phi + X'_{\phi\phi}\phi^2 + X'_{\beta\beta\beta\beta}\beta^4$$
$$Y'_H = Y'_\beta\beta + Y'_\phi\phi + Y'_{\beta\beta\beta}\beta^3 + Y'_{\beta\beta\phi}\beta^2\phi + Y'_{\beta\phi\phi}\beta\phi^2 + Y'_{\phi\phi\phi}\phi^3$$
$$N'_H = N'_\beta\beta + N'_\phi\phi + N'_{\beta\beta\beta}\beta^3 + N'_{\beta\beta\phi}\beta^2\phi + N'_{\beta\phi\phi}\beta\phi^2 + N'_{\phi\phi\phi}\phi^3$$
$$K'_H = K'_\beta\beta + K'_\phi\phi + K'_{\beta\beta\beta}\beta^3 + K'_{\beta\beta\phi}\beta^2\phi + K'_{\beta\phi\phi}\beta\phi^2 + K'_{\phi\phi\phi}\phi^3 \quad (4a)$$

The calm water resistance $X'_0$ corresponds to the first term of $X'_H$. Measured values of $X'_0$ are captured in the polynomial expression using the Froude number $F_n$

$$X'_0 = R_0 + R_1F_n + R_2F_n^2 + R_3F_n^3 \quad (4b)$$

The hydrodynamic derivatives of Eq. 4a and the calm water resistance coefficients of Eq. 4b are provided from model tests undertaken in the small NMRI towing tank (50 m by 8 m by 4.5 m). In the experiments a tanker model with similar $L/B$, $B/d$ and the same block coefficient as the bulk carrier shown in Table 1 was used as the hydrodynamic model. Measured values of the indicated hydrodynamic coefficients for the selected ship model are presented in Table 2.

As demonstrated in Fig. 5 plots of the hydrodynamic forces and moments as a function of the drift angle (–30° to +30° in 2.5° increments for drift angles up to magnitude of 5°, and 5.0° increments for larger drift angles) for different heel angles (0°, 3°, 6° and 9°) indicate that $X'_H$, $Y'_H$ and $N'_H$ are fairly insensitive to changes

**Table 2.** Thrust characteristics, propeller, rudder and sail together with the hydrodynamic derivatives of the ship

| | | Hydro. derivative | |
|---|---|---|---|
| Calm water resistance | | | |
| $R_0$ | 1.16E – 02 | $X'_{\beta\beta}$ | 0.0046 |
| $R_1$ | –1.51E – 02 | $X'_{\beta\varphi}$ | –0.0277 |
| $R_2$ | –1.58E – 01 | $X'_{\varphi\varphi}$ | 0.0176 |
| $R_3$ | 1.14E + 00 | $X'_{\beta\beta\beta\beta}$ | 0.1616 |
| Propeller | | $Y'_\beta$ | 0.2836 |
| $D_P$ (m) | 5.20 | $Y'_\varphi$ | 0.0237 |
| $1 - t_p$ | 0.776 | $Y'_{\beta\beta\beta}$ | 0.6724 |
| $1 - w_{P0}$ | 0.488 | $Y'_{\beta\beta\varphi}$ | 0.3467 |
| $P$ (m) | 3.44 | $Y'_{\beta\varphi\varphi}$ | 1.5391 |
| Rudder | | $Y'_{\varphi\varphi\varphi}$ | –0.6382 |
| $\Lambda$ | 1.70 | $N'_\beta$ | 0.1264 |
| $h$ (m) | 7.00 | $N'_\varphi$ | –0.0225 |
| $1 - t_R$ | 0.775 | $N'_{\beta\beta\beta}$ | –0.0085 |
| $a_H$ | 0.760 | $N'_{\beta\beta\varphi}$ | –0.0379 |
| $x'_H$ | –0.400 | $N'_{\beta\varphi\varphi}$ | –0.0454 |
| $x'_R$ | –0.500 | $N'_{\varphi\varphi\varphi}$ | –0.0775 |
| $z'_R$ | 0.680 | $K'_\beta$ | –0.0312 |
| Sail area and mass | | $K'_\varphi$ | –0.0582 |
| Rec.S (m²) | 614 × 4 | $K'_{\beta\beta\beta}$ | –1.1221 |
| Tri.S (m²) | 393 × 4 | $K'_{\beta\beta\varphi}$ | 2.4186 |
| Rec.$m_{Sa}$ (kg) | 92100 × 4 | $K'_{\beta\varphi\varphi}$ | 1.5020 |
| Tri.$m_{Sa}$ (kg) | 58950 × 4 | $K'_{\varphi\varphi\varphi}$ | 2.5521 |

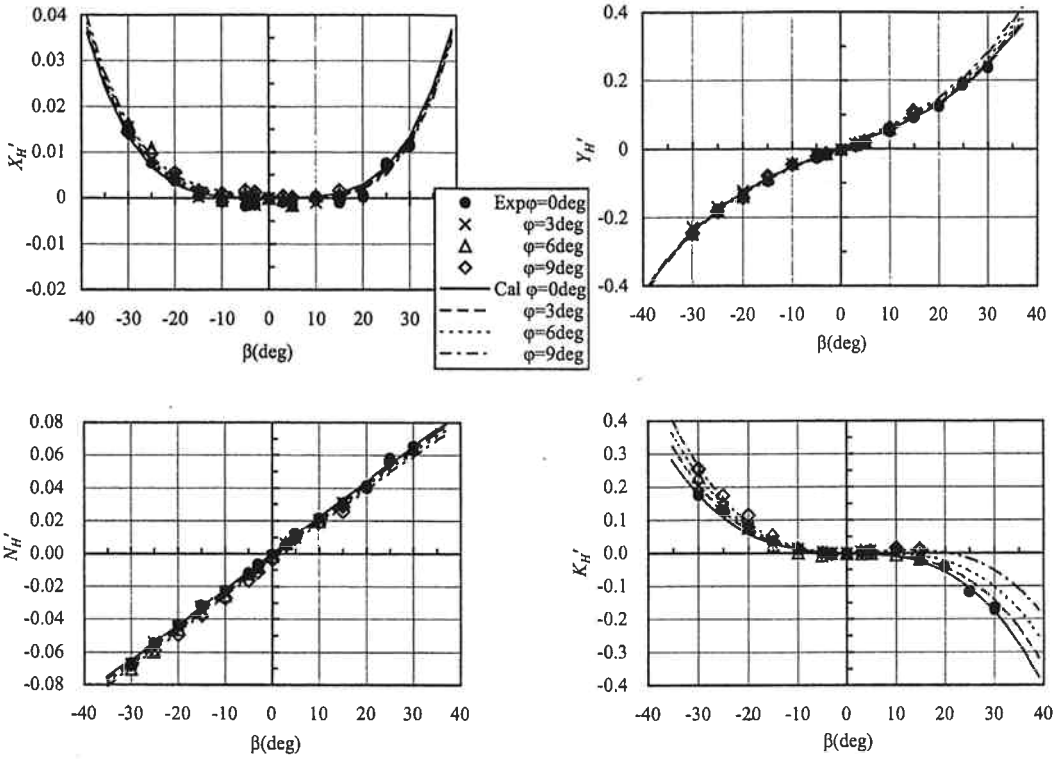


**Fig. 5.** Hull hydrodynamic force and moment coefficients

of heel angle over the complete drift angle range, whilst the heeling moment $K'_H$ is highly sensitive to heel angle variations over all intervals of drift angle. However, the application of the coefficients presented in Table 2 with Eq. 4a predicts hydrodynamic loads that compare well with the measured values. Furthermore, the average multiple correlation coefficient for the regression analysis is 0.991. Similarly, high levels of confidence are associated with the use of Eq. 4b and the $R$ coefficients of Table 2 for calm water resistance, that is, fitted curve and data plots as a function of forward speed are essentially coincident, as illustrated in Fig. 6. Hence the authors are confident that the hydrodynamic load predictors based on applying Eq. 4 with the numerical values of hydrodynamic coefficients of Table 2 capture the hydrodynamic characteristics of the bulk carrier being investigated.

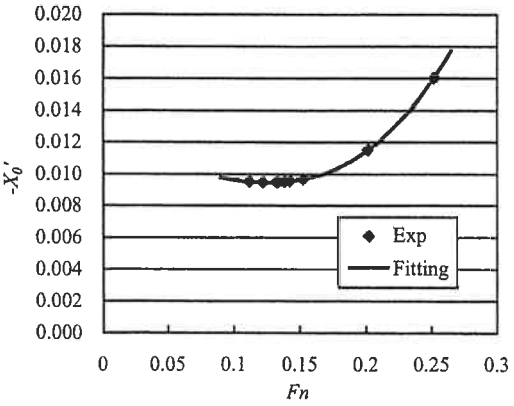


**Fig. 6.** Calm water resistance $X'_0$

*Propeller loads*

The propeller thrust force $X'_P$ is determined in a manner consistent with the MMG model[12] using

$$X'_P = (1-t_P)n^2 D_P^4 K_T(J) \Big/ \frac{1}{2} L_{PP} d U^2 \tag{5a}$$

That is, the propeller thrust is dependent upon the thrust deduction fraction, $t_P$, the rotational velocity of the propeller, $n$, the propeller diameter, $D_P$, and the advance coefficient dependent thrust coefficient $K_T(J)$. The advance coefficient and wake fraction are also defined in accordance with the MMG model. For the steady-state situations to be investigated $J$ has the usual form

$$J = u(1-w_P)/(nD_P) \tag{5b}$$

whereas $w_P$ has the simplified form

$$w_P = w_{P0} \exp(-4.0\beta^2) \tag{5c}$$

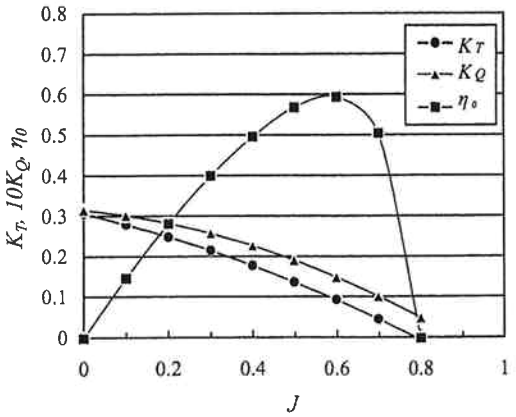


**Fig. 7.** Propeller characteristics used in the calculation

From Fig. 4, it is clear that the surge velocity is given by $u = U\cos\beta$.

The thrust coefficient $K_T(J)$ used in this updated analysis and in the earlier investigations of Minami et al.[9] is provided in Fig. 7. Clearly the propeller revolutions, $n$, need to be selected so that the advance coefficient provides sufficient thrust to attain the required speed of advance $U$. Details of the assumed geometric propeller characteristics, together with the thrust deduction fraction $t_P$ and the wake fraction coefficient $w_{P0}$, selected from tanker data with the same block coefficient, are provided in Table 2.

*Rudder loads*

The rudder forces and moments are defined in terms of the Kijima et al.[1] coefficients $a_H$, $x'_H$ and $t_R$, the rudder orientation, $\delta$, and the associated resultant normal rudder force, $F'_N$. The rudder loads are defined as

$$\begin{aligned} X'_R &= -(1-t_R)F'_N\sin\delta \\ Y'_R &= -(1+a_H)F'_N\cos\delta \\ N'_R &= -(x'_R + a_H x'_H)F'_N\cos\delta \\ K'_R &= -(1+a_H)z'_R F'_N\cos\delta \end{aligned} \qquad (6a)$$

The non-dimensional coordinates $x'_R = x_R/L_{PP}$ and $z'_R = z_R/d$ are associated with the rudder point defined as the intersection of the vertical line through the aft perpendicular and the horizontal line $0.68d$ below the undisturbed free surface. The position of this selected point is defined with respect to the Cartesian reference system origin located at the intersection of the still water plane, the amidships section and the longitudinal plane of ship symmetry.

The Kijima coefficient values for $a_H$ and $x'_H$, presented in Table 2, are dependent upon the block coefficient $C_B$, and are identified from the graphs (for $C_B$ in the range 0.50–0.82) provided as Fig. 1 in Kijima et al.[1] Moreover, $(1 - t_R)$ is obtained using the formula[1]

$$(1-t_R) = 0.28C_B + 0.55 \qquad (6b)$$

The normal rudder force $F'_N$ is defined in terms of the rudder aspect ratio dependent force coefficient $f_A$ derived by Fujii and Tsuda,[2] that is,

$$\begin{aligned} F'_N &= f_A A_R U'^2_R \sin\alpha_R/(L_{PP}d) \quad \text{and} \\ f_A &= 6.13\Lambda/(2.25+\Lambda) \end{aligned} \qquad (6c)$$

The effective flow over the rudder $U'_R$ is determined using the following relationships of Kijima et al.,[1] namely

$$U'^2_R = (1-w_R)^2\left[1+\eta_P k\{2-(2-k)s\}s/(1-s)^2\right] \qquad (6d)$$

with the dependent parameters defined according to

$$\begin{aligned} w_R &= w_P w_{R0}/w_{P0} \equiv w_{R0}\exp(-4.0\beta^2) \quad \text{using Eq. 5c} \\ w_{R0} &= -7.44dC_B/L_{PP} - 2.39C_B B/L_{PP}\cdot\sigma_A + 0.851 \\ \sigma_A &= (1-C_{WA})/(1-C_{PA}) \end{aligned}$$

where

$$\begin{aligned} \eta_P &= D_P/h, \quad \text{and} \quad k = 0.6(1-w_P)/(1-w_R) \\ s &= 1-u(1-w_P)/nP \equiv 1-JD_P/P \quad \text{using Eq. 5b} \end{aligned} \qquad (6e)$$

The inflow angle for the rudder $\alpha_R$ is determined from

$$\alpha_R = \delta - \gamma_R\beta \qquad (6f)$$

subject to the Kijima and Nakiri[14] relationships

$$\begin{aligned} \gamma_R &= 4.02d(1-C_B)/B + 1.98\left[d(1-C_B)/B\cdot e'_A\right]^2 \\ &\quad - 1.54\left[d(1-C_B)/B\cdot e'_A\right] + 0.22 \end{aligned} \qquad (6g)$$

with

$$e'_A = \frac{e_A}{\sqrt{1/4+1/(B/d)^2}} \quad \text{and} \quad e_A = \frac{L_{PP}}{B}(1-C_{PA}) \qquad (6h)$$

The values of the additional coefficients required are provided in Table 2.

*Wind loads*

The non-dimensional wind forces and moments acting on the ship and the sails can either be expressed in terms of the ship steady velocity, that is,

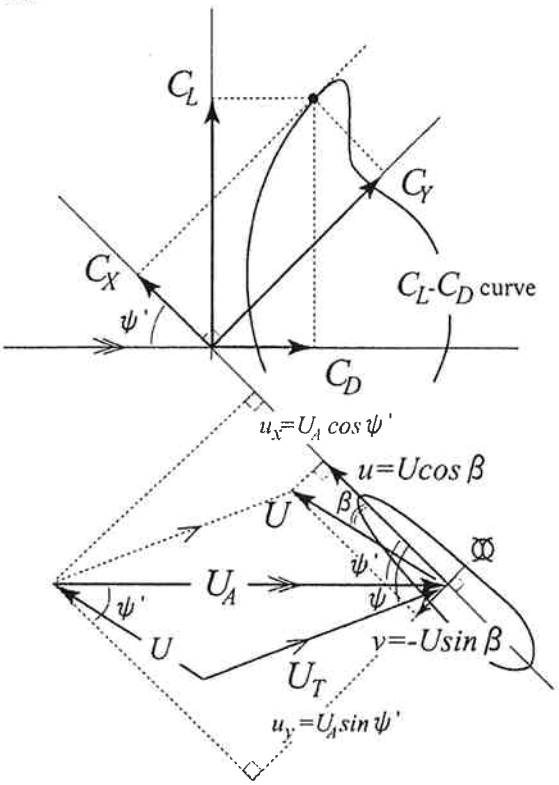


**Fig. 8.** Polar diagram on steady sailing condition for the sail-assisted ship

$$X'_A = X_S \Big/ \left(\frac{\rho}{2} L_{PP} d U^2\right)$$
$$Y'_A = Y_S \Big/ \left(\frac{\rho}{2} L_{PP} d U^2\right)$$
$$N'_A = N_S \Big/ \left(\frac{\rho}{2} L_{PP}^2 d U^2\right)$$
$$K'_A = \left(K_S + Y_S OG\right) \Big/ \left(\frac{\rho}{2} L_{PP} d^2 U^2\right), \qquad (7a)$$

or expressed in terms of the specified relative wind velocity as

$$C_X = X_S \Big/ \left(\frac{\rho_A}{2} U_A^2 A_T\right)$$
$$C_Y = Y_S \Big/ \left(\frac{\rho_A}{2} U_A^2 A_L\right)$$
$$C_N = N_S \Big/ \left(\frac{\rho_A}{2} U_A^2 A_L L_{OA}\right)$$
$$C_K = K_S \Big/ \left(\frac{\rho_A}{2} U_A^2 A_L^2 \Big/ L_{OA}\right). \qquad (7b)$$

Here, $A_T$ and $A_L$ are the transverse and lateral projected areas of the ship, respectively, and exclude the projected area of the sails, $S$.

The wind tunnel data were collected for different headings of the wind relative to the ship. The wind tunnel force coefficients of Eq. 7b apply when the wind velocity and direction ($U_A$, $\psi'$) are specified relative to a stationary ship, that is, using the velocity components defined in Fig. 8 it follows that wind velocity components ($u_x$, $u_y$) satisfy

$$u_x = U_T \cos\psi + U\cos\beta$$
$$u_y = U_T \sin\psi - U\sin\beta, \qquad (7c)$$

with the right-handed Cartesian reference system $x$–$y$ defined with the $x$-axis positive in the direction of $u$ and the $y$-axis positive to starboard. Here, $U_T$ stands for true wind speed. Thus required equivalent resultant wind velocity and heading relative to a stationary ship satisfy

$$U_A^2 = u_x^2 + u_y^2 = U_T^2 + U^2 + 2U_T U\cos(\psi+\beta)$$
$$\psi' = \tan^{-1}\frac{u_x}{u_y} = \tan^{-1}\frac{U_T\cos\psi + U\cos\beta}{U_T\sin\psi - U\sin\beta}. \qquad (7d)$$

That is, to extract the required wind coefficients from Figs. 9 and 10 one simply uses $\psi'$ defined in Eq. 7d and selects $C_X$, $C_Y$ and $C_N$, $C_K$ for the experimental condition of interest. The calculated apparent wind velocity $U_A$ is then used with Eq. 7b to determine the dimensional forces and moments required to provide the non-dimensional wind coefficients expressed in Eq. 7a, in readiness for ultimate substitution into the generic force and moment expressions of Eq. 2.

It should be noted that the angles associated with the setting of the hybrid-sail are not referenced explicitly since the wind force and wind moment coefficients were determined subject to the parallel, graduated or goose-wing setting being organised to produce maximal driving force. The settings of the sails in each case have been noted, but their values are not required in this steady-state analysis.

The values of the wind loading coefficients defined in Eq. 7b are presented in Figs. 9 and 10 for the rectangular and triangular soft sail arrangements of the hybrid-sail, respectively, together with the corresponding coefficient values for the ship without any sails. The with-sails data[10,11] of Figs. 9 and 10 cover three distinct situations.

1. A single isolated sail is investigated and the resulting polar diagram is used to provide the total wind loading on a set of four sails without sail–sail interactions. The wind load on the ship without sails is then

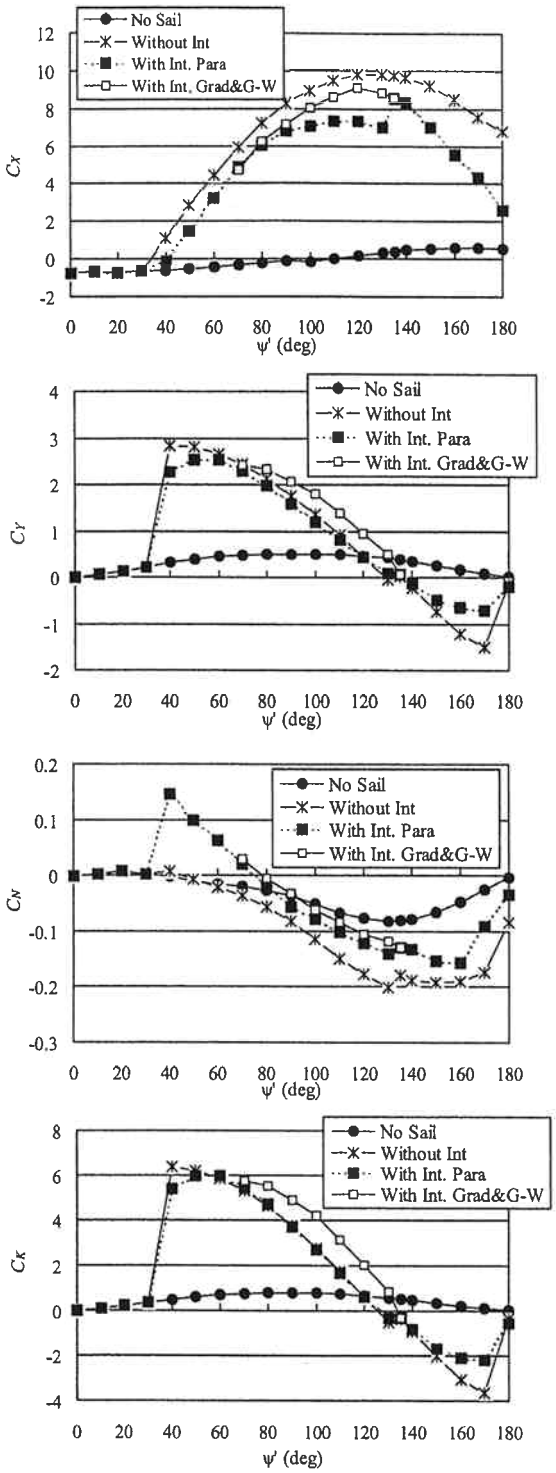


**Fig. 9.** Wind dependent hull forces and moments, with and without the interaction effects of rectangular sails, for different experimental arrangements

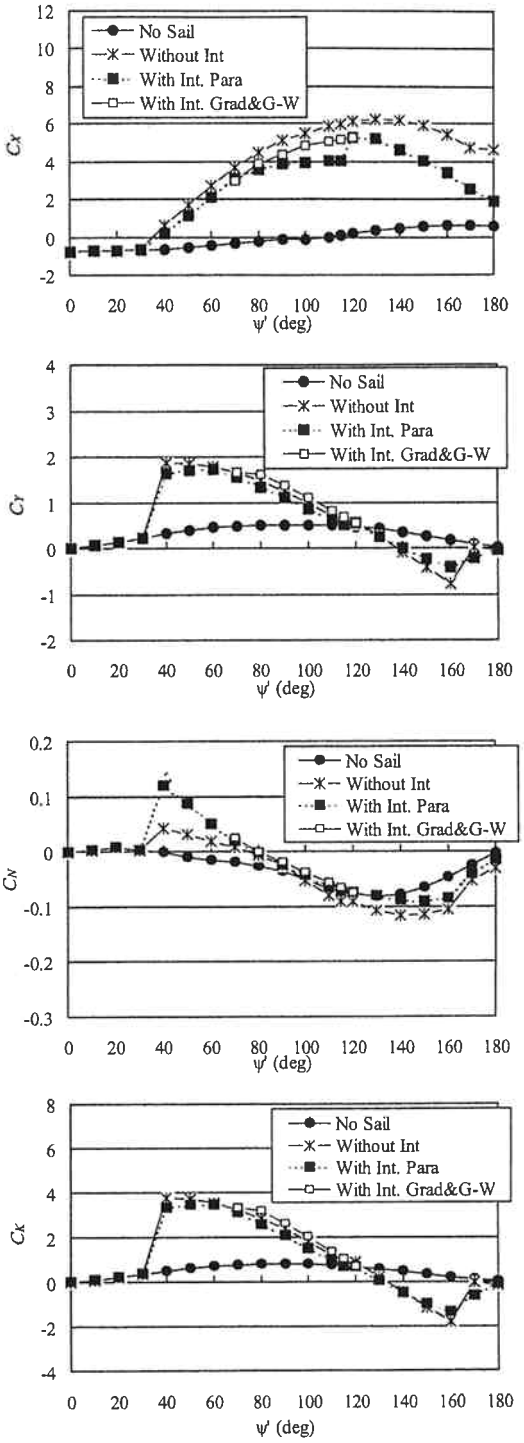


**Fig. 10.** Wind dependent hull forces and moments, with and without the interaction effects of triangular sails, for different experimental arrangements

included without any sail–hull interaction effects. In cited figures, this combined wind load is designated "Without Int."

2. A set of sails installed on a ship model and wind tunnel tests carried out with a set of 4 hybrid-sails set parallel to each other for a ship model draught corresponding to the fully-loaded condition. The situation is denoted "With Int. Para" in the legends of the figures cited.
3. Sails and a ship model investigated with sails set in either the near optimum non-parallel condition

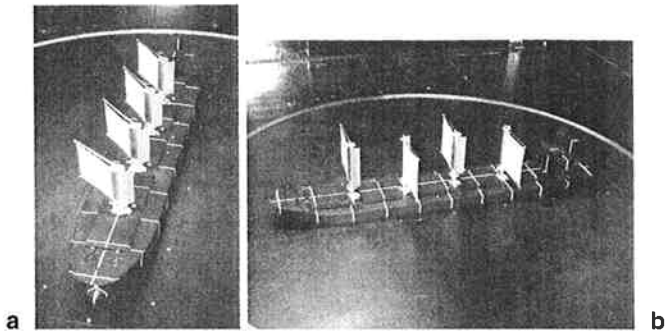


**Fig. 11.** Photographs of the bulk carrier model with sail arrangements (**a**) graduated and (**b**) goose-winged

designated the "graduated arrangement" or set in the "goose-winged" arrangement in Fig. 11. The "graduated arrangement" of the sails is fully explained by Fujiwara et al.[11] In this case the figure legend "With Int. Grad & G-W" describes experimental conditions.

## Calculated results

The equilibrium equations of Eq. 2 are modified in accordance with the external load equations of Eq. 3 using the different hydrodynamic and aerodynamic loads defined in Eqs. 4–7. The resulting nonlinear algebraic equations are then solved for the unknown variables $U$, $\beta$, $\phi$ and $\delta$ using the multi-variable Newton–Raphson method.

If the engine settings remain fixed when the steady-state ship motion equations are examined, with and without sails, the speed of advance is likely to exceed the preferred cruising speed when sails are deployed. Therefore the equations are solved with the engine revolutions fixed (at a level to attain the required speed without sail assistance) to appreciate the increase in speed the sails provide, and then solved under the conditions that the engine revolutions are set to maintain the designed cruising speed, for example, 13.5 knots. In the first case the Newton–Raphson method is applied in a straightforward manner, whereas in the second case the setting of the engine revolutions, $n$, is modified using the Newton method (exploiting linear interpolation to accelerate the convergence process) until engine revolutions for selected wind conditions yield the required cruising speed.

### *Interaction effect for the sailing performance*

The calculated results for $U$, $\beta$, $\phi$ and $\delta$ in the steady sailing condition $U_T$ = 15 m/s and different wind directions, $\psi$, are shown in Fig. 12 for a parallel setting of the

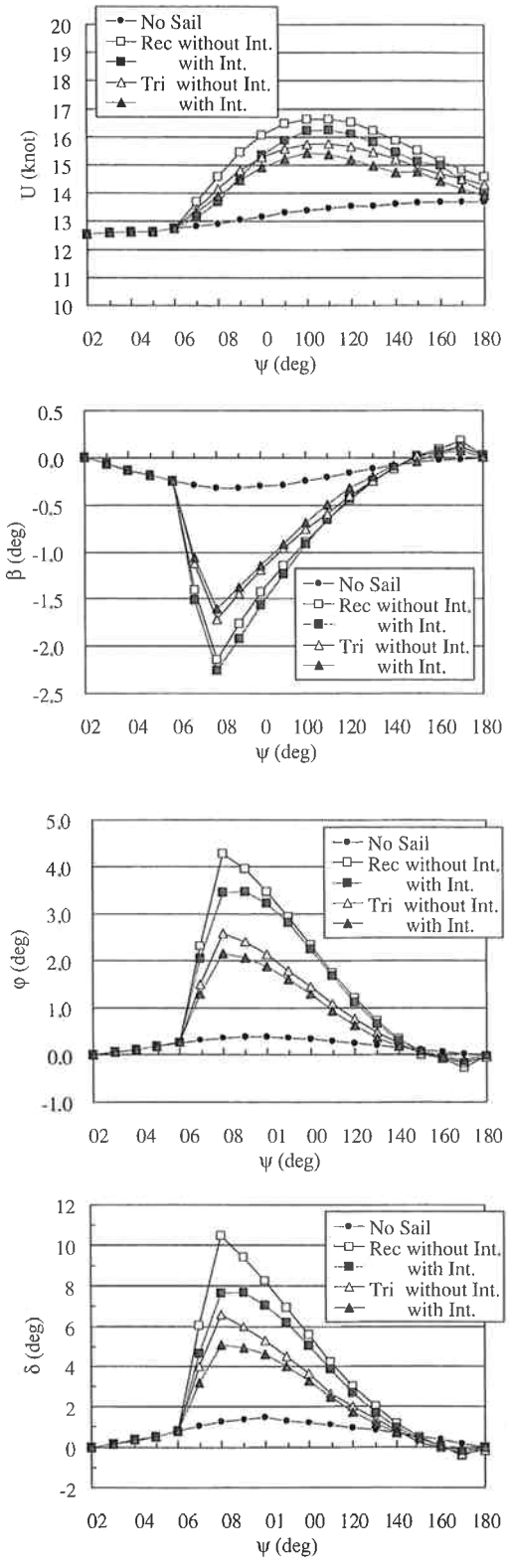


**Fig. 12.** Calculated ship characteristics for steady sailing conditions for parallel sail conditions on rectangular and triangular sails and fixed wind speed ($U_T$ = 15 m/s, $n$ = 2.07 rps)

four sails, subject to the preferred sail-setting condition of $\xi = 35°$ and $\gamma = 30°$ (see Fig. 3). In the case of no-wind condition, the ship is able to maintain a steady speed of advance 13.5 knots when the rotational velocity of the propeller is held constant at 2.07 rps.

The values of $U$, $\beta$, $\phi$ and $\delta$ are different when comparing the steady no-sail condition predictions with those of the with-sail situation. The effect of the sail–sail and sail–hull interactions has its greatest influence upon the parameters $U$, $\phi$ and $\delta$, but such interaction effects have their greatest influence when the ship is sailing close-hauled or the ship is subject to beam winds. In the wind range $\psi = 160°$ to $\psi = 180°$ the effect of interactions is minimal, despite the strong interaction effects on the individual sail drive forces shown in Figs. 9 and 10. This observation is reasonable because the relative wind velocity becomes very small for these wind directions and so the lack of apparent sail driving force is not so important.

Moreover, the fact that $\phi$ is generally less than 5° on rectangular sails and 3° on triangular sails suggests that the sails do not have an adverse influence on the ship. The higher levels of heel are in fact associated with the without-interaction model. The interaction effects lower the maximum heel angle to 3.5° for rectangular sails and to 2.2° for triangular sails. These solutions are considered to be more realistic in terms of real sailing conditions.

### *Steady-sailing condition in the case of constant ship speed*

If the sail settings are based on the graduated or goose-winged arrangement, the derived solutions for $n$, $\beta$, $\phi$ and $\delta$ with interaction effects are provided in Fig. 13 for rectangular sails, and in Fig. 14 for triangular sails subject to $U$ being maintained at the constant operational speed of 13.5 knots in different wind conditions.

Each value for $n$, $\beta$, $\phi$ and $\delta$ on the rectangular soft sail system is more different than that on the triangular soft sail system. From Fig. 12, when $U_T$ = 15 m/s, one can deduce that the variations in the determined quantities of Figs. 13 and 14 are large compared with the expected variations for $U_T$ = 0 m/s for which $\beta$, $\phi$, $\delta$ will be essentially zero and $n$ fixed at 2.07 rps. The results in Figs. 13 and 14 indicate that the absolute values of $\beta$, $\phi$ and $\delta$ become larger with increased wind velocity and furthermore their maximum values correspond to smaller true wind directions as the wind velocity increases. However, $n$ becomes smaller as the wind velocity increases. For a small range of $\psi$ values for $U_T$ = 17.5 m/s the propeller revolutions cannot be meaningfully reduced for the rectangular sails. For this velocity and wind direction range the ship would in fact travel faster than the desired speed of 13.5 knots (since

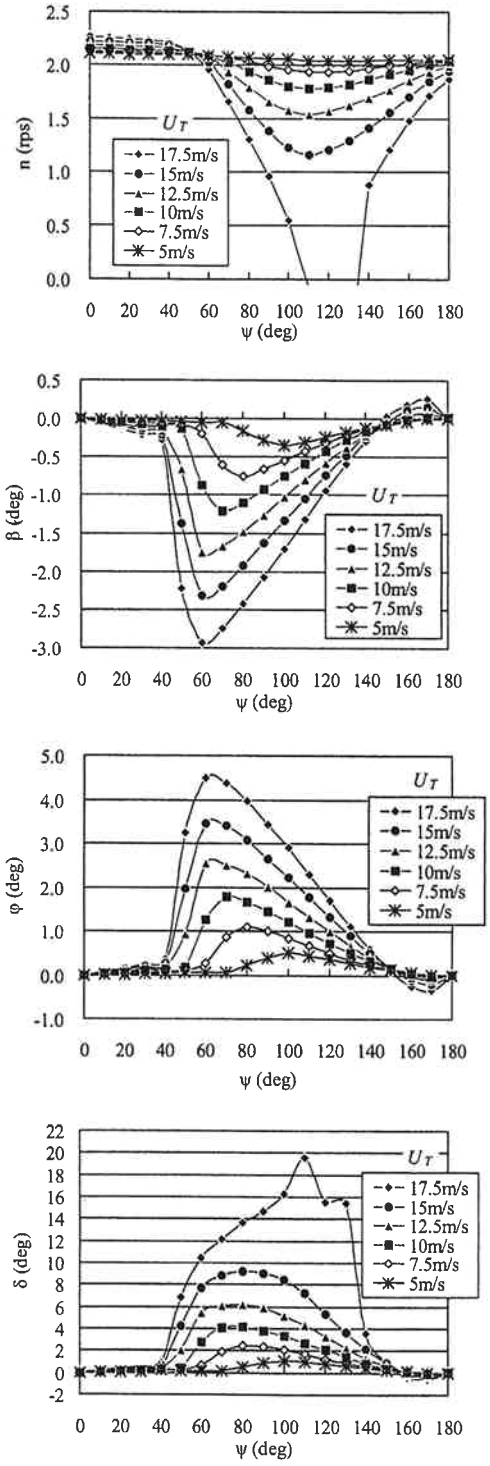


**Fig. 13.** Calculated ship characteristics for different wind speeds and fixed speed of ship advance in the case of rectangular sails for graduated and goose-winged sail configuration ($U$ = 13.5 knots)

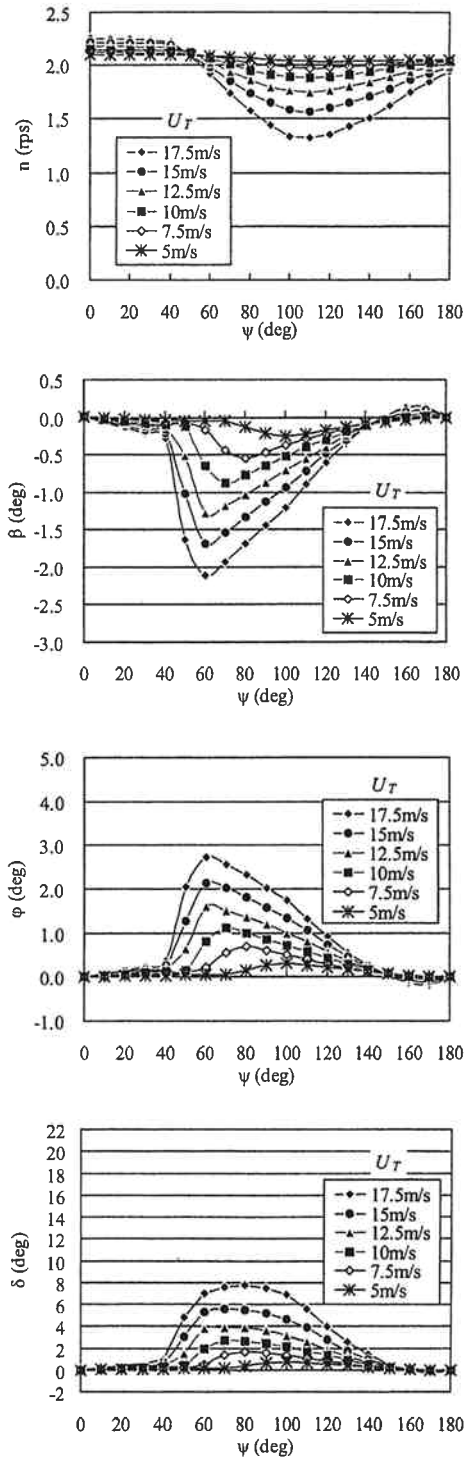


**Fig. 14.** Calculated ship characteristics for different wind speeds and fixed speed of ship advance in the case of triangular sails for graduated and goose-winged sail configuration ($U$ = 13.5 knots)

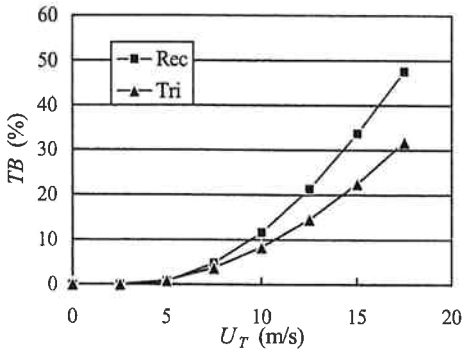


**Fig. 15.** Thrust benefit for different wind speeds for fixed speed of ship advance and graduated and goose-winged sail configuration ($U$ = 13.5 knots)

otherwise physically meaningless negative $n$ values are required) and the rudder angle also exhibits an unnatural local peak.

The heel angle $\phi$ is less than 4.5° for the rectangular sails and 2.8° for the triangular sails when $U_T$ = 17.5 m/s. For all wind speeds and wind angles, the heel angle is not particularly large. Hence, although bulk carriers do not have a keel or centerboard, like a yacht, the results presented indicate that the bulk carrier can operate successfully with sails.

### *Assessment of sail-assisted ship benefits*

#### *Thrust reduction in the case of U = 13.5 knots*

The thrust benefit (TB) concept is introduced to provide a measure of the ability of the sails to reduce the engine delivered thrust subject to maintaining the required speed of advance. The TB metric is expressed as a percentage and defined in accordance with

$$\mathrm{TB}(\%) = \frac{\overline{X}_{\mathrm{P(nosail)}} - \overline{X}_{\mathrm{P(withsails)}}}{\overline{X}_{\mathrm{P(nosail)}}} \times 100 \qquad (8)$$

In Eq. 8, $\overline{X}_{\mathrm{P(nosail)}}$ represents the mean value of the thrust force for the ship without the sails for all wind directions, whereas $\overline{X}_{\mathrm{P(withsails)}}$ is the mean value of the thrust force when the sails assume a graduated or goose-wing arrangement and the same constant ship velocity of $U$ = 13.5 knots is maintained. Thus TB is equivalent to a mean reduction in effective horse power (EHP). Having observed that graduated and goose-winged sail configurations can reduce the negative aspects of sail–hull interactions the influence of wind speed upon thrust benefit is presented in Fig. 15.

In the case of $U_T$ = 5 m/s, the thrust benefit is expected to be very small because wind velocity and ship velocity are of comparable magnitudes. However, in the case of $U_T$ = 10 m/s the ship with the rectangular sails can gain

**Table 3.** BHP for different wind angles and speeds for fixed speed of ship advance ($U$ = 13.5 knots) and graduated and goose-winged sail configurations

| | $U_T$ = 10 m/s | | | $U_T$ = 15 m/s | | |
|---|---|---|---|---|---|---|
| $\psi$ | No sail | Rec | Tri | No sail | Rec | Tri |
| 0 | 8.65E + 03 | 8.66E + 03 | 8.65E + 03 | 9.61E + 03 | 9.61E + 03 | 9.61E + 03 |
| 10 | 8.60E + 03 | 8.60E + 03 | 8.60E + 03 | 9.50E + 03 | 9.50E + 03 | 9.50E + 03 |
| 20 | 8.54E + 03 | 8.54E + 03 | 8.54E + 03 | 9.44E + 03 | 9.44E + 03 | 9.44E + 03 |
| 30 | 8.52E + 03 | 8.52E + 03 | 8.52E + 03 | 9.39E + 03 | 9.39E + 03 | 9.39E + 03 |
| 40 | 8.41E + 03 | 8.41E + 03 | 8.41E + 03 | 9.13E + 03 | 9.13E + 03 | 9.13E + 03 |
| 50 | 8.26E + 03 | 8.26E + 03 | 8.26E + 03 | 8.99E + 03 | 8.37E + 03 | 7.97E + 03 |
| 60 | 8.19E + 03 | 7.75E + 03 | 7.51E + 03 | 8.83E + 03 | 7.02E + 03 | 6.55E + 03 |
| 70 | 8.07E + 03 | 7.03E + 03 | 6.84E + 03 | 8.51E + 03 | 4.88E + 03 | 4.20E + 03 |
| 80 | 7.90E + 03 | 6.06E + 03 | 6.26E + 03 | 8.22E + 03 | 3.00E + 03 | 4.18E + 03 |
| 90 | 7.75E + 03 | 5.26E + 03 | 5.85E + 03 | 7.95E + 03 | 1.84E + 03 | 3.49E + 03 |
| 100 | 7.61E + 03 | 4.77E + 03 | 5.62E + 03 | 7.72E + 03 | 1.16E + 03 | 3.05E + 03 |
| 110 | 7.50E + 03 | 4.59E + 03 | 5.54E + 03 | 7.54E + 03 | 8.96E + 03 | 2.91E + 03 |
| 120 | 7.41E + 03 | 4.62E + 03 | 5.60E + 03 | 7.43E + 03 | 1.08E + 03 | 3.14E + 03 |
| 130 | 7.35E + 03 | 4.94E + 03 | 5.83E + 03 | 7.39E + 03 | 1.43E + 03 | 3.49E + 03 |
| 140 | 7.33E + 03 | 5.38E + 03 | 6.12E + 03 | 7.23E + 03 | 2.00E + 03 | 3.97E + 03 |
| 150 | 7.30E + 03 | 5.87E + 03 | 6.45E + 03 | 7.11E + 03 | 2.83E + 03 | 4.50E + 03 |
| 160 | 7.26E + 03 | 6.34E + 03 | 6.73E + 03 | 7.05E + 03 | 3.92E + 03 | 5.31E + 03 |
| 170 | 7.25E + 03 | 6.80E + 03 | 7.01E + 03 | 7.04E + 03 | 5.16E + 03 | 5.96E + 03 |
| 180 | 7.26E + 03 | 7.13E + 03 | 7.19E + 03 | 7.07E + 03 | 6.15E + 03 | 6.60E + 03 |
| $\overline{\text{BHP}}$ | 7.85E + 03 | 6.71E + 03 | 7.03E + 03 | 8.17E + 03 | 5.10E + 03 | 5.97E + 03 |

11.7% of the required thrust from the hybrid-sails, and in the case of $U_T$ = 15 m/s a gain of 33.8% is attained. The corresponding values in the case of triangular soft sails are 8.3% for $U_T$ = 10 m/s and 22.6% for $U_T$ = 15 m/s. Thus the thrust generated by the main engines can be reduced by the positive effect of the sails presence.

*Expected reduction in BHP and FOC when operating in the North Pacific Ocean*

Many Japanese bulk carriers operate in the North Pacific Ocean. In this sea area Watanabe et al.[15] have established a wind database. The benefit of the sail-assisted ship, expressed in terms of brake horse power (BHP), is investigated by using the cited database. For example, the BHP values in the case of a sail-assisted ship operating in the North Pacific Ocean at U = 13.5 knots, for the ship without sails "No Sail", with rectangular soft sails and with triangular sails are provided in Table 3. The expected value (EV) of the reduced BHP is obtained using the equations

$$\text{DHP} = 2\pi K_Q(J)\rho n^3 D_P^5/735.5 \tag{9}$$

$$\begin{aligned}\overline{\text{BHP}}(U,U_T)\Big|_{\text{nosail}}^{\text{withsails}} &= \frac{1}{N_A}\sum_{i=1}^{N_A}\text{BHP}(U,U_T,\psi_i)\Big|_{\text{nosail}}^{\text{withsails}} \\ &= \frac{1}{N_A}\sum_{i=1}^{N_A}\frac{\eta_{QC}}{\eta_{PC}}\text{DHP}(U,U_T,\psi_i)\Big|_{\text{nosail}}^{\text{withsails}} \\ &= \frac{1}{N_A}\sum_{i=1}^{N_A}1.03\text{DHP}(U,U_T,\psi_i)\Big|_{\text{nosail}}^{\text{withsails}}\end{aligned} \tag{10}$$

$$\begin{aligned}\Delta\overline{\text{BHP}}_{\text{EV}}(U) &\equiv E\left[\Delta\overline{\text{BHP}}(U,U_T)\right] \\ &= \sum_{i=1}^{N_P}P_{U_{T_i}}\left(\overline{\text{BHP}}(U,U_T)_{\text{nosail}}\right. \\ &\quad \left. - \overline{\text{BHP}}(U,U_T)_{\text{withsails}}\right)\end{aligned} \tag{11}$$

Here, DHP, $\eta_{QC}$, $\eta_{PC}$ are the delivered horsepower, the quasi-propulsive and propulsive coefficient, respectively. The ratio of propulsive coefficient, $\eta_{QC}/\eta_{PC}$, is assumed to be 1.03. The torque coefficient $K_Q(J)$ is shown in Fig. 7. The number of true wind directions (measured relative to the ship) is $N_A$. In the calculation $\psi_i$ will vary from 0°, in increments of 10°, up to a wind heading of 180°. The probability of the wind velocity $P_{U_T}$ is obtained from the database of the North Pacific Ocean. Here, the number of discrete wind ranges, $N_P$, is set to 5. In the case of $U$ = 13.5 knots, the EV of the reduced BHP of the ship is 961 ps and 714 ps for the rectangular and triangular sails, respectively (see Table 4). In the analysis, it is assumed that sail operation ceases with $U_T \geq 20.0$ m/s. For such wind speeds the soft sails are considered to be at risk in terms of structural integrity and would be withdrawn from service.

The BHP difference ratio is defined as the ratio of $\overline{\text{BHP}}(U, U_T)_{\text{withsails}}$ to $\overline{\text{BHP}}(U, U_T)_{\text{nosail}}$. This is effectively measured using the expression

**Table 4.** Expected values of the reduced BHP for a fixed speed of ship advance in navigating the North Pacific Ocean, for rectangular and triangular sails with graduated and goose-winged sail configurations ($U = 13.5$ knots)

| Wind $U_T$ | | | No sail | | Rectangular sails | | | Triangular sails | | |
|---|---|---|---|---|---|---|---|---|---|---|
| Range (m/s) | Represent (m/s) | $P_{U_T}$ (%) (a) | $\overline{BHP}$ (ps) (b) | $\overline{BHP}'$ (ps) (a) × (b) | $\overline{BHP}$ (ps) (c) | $\Delta\overline{BHP}$ (ps) (d) = (b) − (c) | $\Delta\overline{BHP}'$ (ps) (a) × (d) | $\overline{BHP}$ (ps) (e) | $\Delta\overline{BHP}$ (ps) (f) = (b) − (e) | $\Delta\overline{BHP}'$ (ps) (a) × (f) |
| 0–5 | 2.5 | 22.57 | 7538 | 1702 | 7538 | 0 | 0 | 7538 | 0 | 0 |
| 5–10 | 7.5 | 45.65 | 7718 | 3523 | 7242 | 475 | 217 | 7343 | 375 | 171 |
| 10–15 | 12.5 | 23.29 | 8002 | 1864 | 5969 | 2033 | 474 | 6557 | 1445 | 337 |
| 15–20 | 17.5 | 6.80 | 8344 | 567 | 4364 | 3980 | 270 | 5313 | 3031 | 206 |
| 20–25 | 22.5 | 1.39 | 8760 | 121 | 8760 | 0 | 0 | 8760 | 0 | 0 |
| Total | — | 99.70 | — | 7777 | — | 6489 | 961 | — | 4851 | 714 |

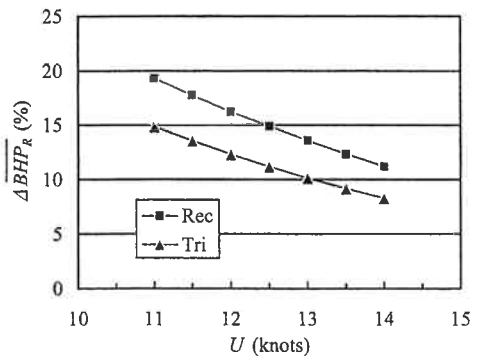


**Fig. 16.** Expected values of reduced BHP depending on speed of ship advance, for rectangular and triangular sails for graduated and goose-winged sail configuration

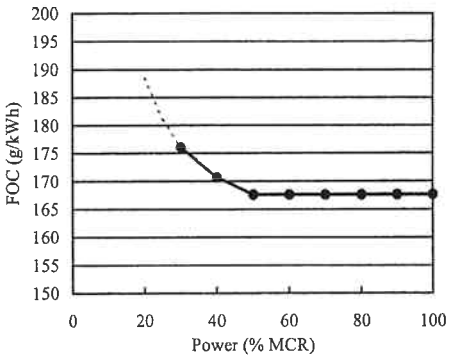


**Fig. 17.** Fuel oil consumption of a sample low speed diesel engine

$$\Delta\overline{\mathrm{BHP}}_{\mathrm{R}}(U) = \frac{\Delta\overline{\mathrm{BHP}}_{\mathrm{EV}}(U)}{\sum_{i=1}^{N_P} P_{U_{T_i}}\,\overline{\mathrm{BHP}}_{\mathrm{nosail}}(U, U_{\mathrm{T}})} \times 100 \qquad (12)$$

The calculated values of $\Delta\overline{\mathrm{BHP}}_{\mathrm{R}}(U)$ as a function of $U$ are provided in Fig. 16 for rectangular and triangular soft sails. The hybrid-sails are set to the graduated and goose-winged arrangements according to wind direction. When the ship speed is lower, the expected value of BHP gained from the hybrid-sails is a higher percentage of the expected value of $\overline{\mathrm{BHP}}(U, U_{\mathrm{T}})_{\mathrm{no\ sail}}$. That is the proportion of machinery generated drive force is reduced. From Table 4, generated for the ship cruising speed $U = 13.5$ knots, $\Delta\overline{\mathrm{BHP}}_{\mathrm{R}}(U)$ is determined from the ratio of 961 to 7777, i.e., 12.4% for rectangular sails, and $\Delta\overline{\mathrm{BHP}}_{\mathrm{R}}(U)$ is determined from the ratio 714 to 7777, i.e., 9.2% for triangular sails. In the case of $U = 11$ knots, corresponding calculations indicate a 19.3% benefit for rectangular sails and a 14.8% benefit for triangular sails. Clearly the rectangular soft sail is more beneficial than the triangular soft sail. The average BHP gain for rectangular sails is of the order of 15.0%.

Having indicated that BHP is reduced as a consequence of sail-assistance, the economic metric of reduced fuel oil consumption is addressed next. The BHP of the bulk carrier subject to no waves, no wind and no sails, at a cruising speed $U$ is defined as 85% of maximum continuous rating (MCR). That is,

$$\mathrm{MCR} = \mathrm{BHP}\left(U \middle| \text{nowind, nowaves, nosails}\right) \times \frac{100}{85} \qquad (13)$$

The fuel oil consumption (FOC) of a low-speed diesel engine as a function of BHP, expressed as a percentage of MCR, has a form similar to that illustrated in Fig. 17. This figure represents a simplified version of Fig. 12.8 in Woud and Stapersma,[16] in which it has been assumed that FOC cannot be reduced below the FOC value associated with the minimum power demand of 30% MCR. To appreciate the sensitivity of FOC to the operational minimum power level, this threshold is also set at 50% MCR in the calculations that follow. A 50% MCR limitation level is typical for a low-speed diesel engine whereas a 30% MCR limitation is an acceptable value in the case of using a new type of diesel engine, for example, a common rail-type engine.

The mean level of FOC averaged over all possible wind directions (with sails and without sails) is determined in accordance with

$$\overline{\mathrm{FOC}}(U,U_\mathrm{T})\Big|_{\text{nosail}}^{\text{withsails}} = \frac{1}{N_\mathrm{A}}\sum_{i=1}^{N_\mathrm{A}}\left[\mathrm{BHP}(U,U_\mathrm{T},\psi_i)\Big|_{\text{nosail}}^{\text{withsails}} \times \mathrm{FOC}\left(\frac{\mathrm{BHP}\Big|_{\text{nosail}}^{\text{withsails}}}{\mathrm{MCR}}\times 100\right)\right] \quad (14)$$

The expected value of the FOC differential and its difference ratio is determined in a manner analogous to the calculation of $\Delta\overline{\mathrm{BHP}}_{\mathrm{EV}}$ and $\Delta\overline{\mathrm{BHP}}_{\mathrm{R}}$. That is,

$$\Delta\overline{\mathrm{FOC}}_{\mathrm{EV}}(U) = \sum_{i=1}^{N_\mathrm{P}} P_{U_{T_i}}\left(\overline{\mathrm{FOC}}_{\text{nosail}}(U,U_\mathrm{T}) - \overline{\mathrm{FOC}}_{\text{withsails}}(U,U_\mathrm{T})\right) \quad (15)$$

and

$$\Delta\overline{\mathrm{FOC}}_{\mathrm{R}}(U) = \frac{\Delta\overline{\mathrm{FOC}}_{\mathrm{EV}}(U)}{\sum_{i=1}^{N_\mathrm{P}} P_{U_{T_i}}\overline{\mathrm{FOC}}_{\text{nosail}}(U,U_\mathrm{T})}\times 100 \quad (16)$$

The calculated results for $\Delta\overline{\mathrm{FOC}}_{\mathrm{R}}(U)$ when the rectangular and triangular sails are set in the graduated and goose-winged arrangements are shown in Fig. 18. $\Delta\overline{\mathrm{FOC}}_{\mathrm{R}}(U)$ is influenced by the setting of the minimum allowable MCR and the selected ship speed. In the case of rectangular sails, $\Delta\overline{\mathrm{FOC}}_{\mathrm{R}}(U)$ for a 30% MCR limitation is on average 3% higher than that of $\Delta\overline{\mathrm{FOC}}_{\mathrm{R}}(U)$ for a 50% MCR limitation. In the case of triangular sails, a 30% MCR limitation at a ship speed of $U = 11$ knots provides the same level of $\Delta\overline{\mathrm{FOC}}_{\mathrm{R}}(U)$ as for rectangular sails with a 50% MCR limitation. On the other hand, in the case of $U = 14$ knots, the values of $\Delta\overline{\mathrm{FOC}}_{\mathrm{R}}(U)$ for triangular sails with a 30% MCR limitation and a 50% MCR limitation are at the same level. Clearly, an appreciation of the allowable MCR limitation is a very important factor when planning sail-assisted ships. The mean value of $\Delta\overline{\mathrm{FOC}}_{\mathrm{R}}(U)$ is approximately 13.3% for rectangular sails with a 30% MCR limitation. This level of fuel oil saving should readily provide the required capital investment for the provision and installation of the hybrid-sail together with an appreciable reduction in operational costs. If a different FOC curve were used (as a consequence of selecting a different type of engine) the changes in $\Delta\overline{\mathrm{FOC}}_{\mathrm{R}}(U)$ would most probably be higher, since the selected FOC curve corresponds to the least fuel demanding engine type.[16]

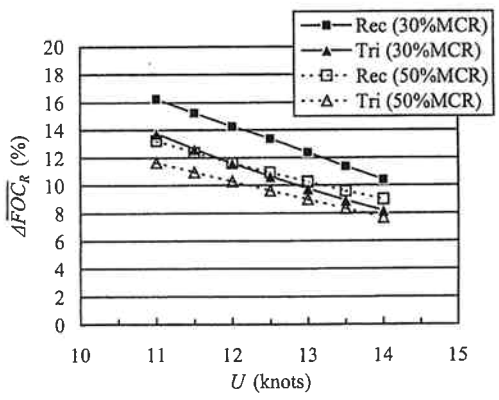


**Fig. 18.** Fuel oil consumption differential depending on ship speed and MCR

## Conclusions

The steady-state effects of a bulk carrier ship with a new type of hybrid-sails were investigated in detail using the MMG simulation method with the experimentally determined key hydrodynamic and aerodynamic coefficients set out in Table 2 and Figs. 5, 6, 9 and 10 together with the propeller characteristics of Fig. 7. The steady-state analysis presented suggests that an appreciation of the sail–sail and sail–hull interaction effects is important in the design of an efficient sail-assisted ship. The effects of the sail form, i.e., rectangular or triangular type hybrid-sails that influences the steady-state sailing performance, were clearly understood. This analysis demonstrated the advantage of the use of rectangular sails. Moreover the benefits of the sail-assisted bulk carrier ship for an expected reduction of BHP and FOC when operating in North Pacific Ocean were presented. The results of the investigation are summarized below.

1. From the steady-state sailing condition based simulations the loss in useful sail generated thrust, as a consequence of sail–sail and sail–hull interactions for the rectangular and triangular type hybrid-sails, see Figs. 9 and 10, is not as significant as the large decrease in thrust on the individual sails shown in Figs. 24 and 25 of Fujiwara et al.[11] Hence whilst sail–sail and sail–hull interactions need to be appreciated, looking at the wind driving forces of sails in isolation, rather than within the context of a contributing force

to the overall dynamics of the ship, can lead to an unnecessarily negative interpretation of sail assistance from the viewpoint of ship operation.
2. While bulk carriers do not have a keel or centreboard, like a yacht, to counter balance the wind heeling moment, the steady-state sailing calculations presented indicate that the bulk carrier can operate successfully with hybrid-sails.
3. In the case of $U_T = 10$ m/s the bulk carrier designed cruising speed, $U = 13.5$ knots, with rectangular type hybrid-sails gains 11.7% of the required thrust from the sails. For the triangular type hybrid-sails gain is 8.3%. These gains increase with increasing wind speed (see Fig. 15).
4. Using North Pacific Ocean wind statistics the calculated BHP results for sails set in the graduated and goose-winged arrangement for $U = 13.5$ knots indicate that the expected value of BHP gain from the hybrid-sails is 12.4% for rectangular type sails and 9.2% for triangular sails.
5. From the analysis of fuel consumption, the expected value of the reduced fuel oil consumption is of the order of 16% when operating at $U = 11$ knots with a 30% MCR limitation. Higher MCR limitation will reduce the fuel consumption benefit to an average level of 13.3% for the preferred rectangular soft sails.
6. The combined experimental and theoretical analyses suggest that realizable benefits in a reduced machine generated driving force and fuel oil consumption can be achieved at a level capable of justifying sail-assisted operations with potential financial savings in operational costs.

## References


1. Kijima K, Katsuno T, Nakiri Y, et al (1990) On the manoeuvring performance of a ship with the parameter of loading condition. J Soc Nav Archit Jpn 168:141–148
2. Fujii H, Tsuda T (1961) Experimental research on rudder performance. 2 (in Japanese). J Soc Nav Archit Jpn 110:31
3. Yoshimura Y, Tanabe Y, Ohsugi I, et al (1990) On the prediction of the sailing performance for a large sail training ship (in Japanese). J Jpn Inst Navig 84:19–27
4. Fujiwara T, Hirata K, Ueno M, et al (2003) On aerodynamic characteristics of a hybrid-sail with square soft sail. In: Proceedings of the International Society of Offshore and Polar Engineering, ISOPE2003, Hawaii, pp 326–333
5. Fujiwara T, Hirata K, Ueno M, et al (2003) On development of high performance sails for an oceangoing sailing ship. In: Proceedings of the International Conference on Marine Simulation and Ship Manoeuvrability, MARSIM'03, Kanazawa, pp RC-23-1-9
6. Ishihara M, Watanabe T, Shimizu K, et al (1980) Prospect of sail-equipped motorship as assessed from experimental ship "*Daioh*". In: Proceedings of the Shipboard Energy Conservation Symposium, Society of Naval Architects and Marine Engineers, pp 181–198
7. Matsumoto N, Inoue M, Sudo M (1982) Operating performance of a sail equipped tanker in wave and wind. In: 2nd International Conference on Stability of Ships and Ocean Vehicles, STAB '82, Tokyo, pp 451–464
8. Minami Y, Nimura T, Fujiwara T, et al (2003) Investigation into underwater fin arrangement effect on steady sailing characteristics of a sail assisted ship. In: Proceedings of the International Society of Offshore and Polar Engineering, ISOPE2003, Hawaii, pp 318–325
9. Minami Y, Nimura T, Fujiwara T, et al (2003) Investigation into underwater fin arrangement effect on steady sailing characteristics of a sail assisted ship. In: Proceedings of the International Conference on Marine Simulation and Ship Manoeuvrability, MARSIM'03, Kanazawa, pp RB-8-1-8
10. Fujiwara T, Kitamura F, Ueno M, et al (2004) Hybrid-sail–hull and sail-sail interaction effects for an ocean-going sailing ship. In: Proceedings of the International Society of Offshore and Polar Engineering, ISOPE2004, Toulon, pp 351–358
11. Fujiwara T, Hearn GE, Kitamura F, et al (2005) Sail–sail and sail–hull interaction effects of hybrid-sail assisted bulk carrier. J Mar Sci Technol 10:82–95
12. Hirano M, Takashina J (1980) A calculation of ship turning motion taking coupling effect due to heel into consideration. J West Jpn Soc Nav Archit 59
13. Kansai Shipbuilding Design Handbook (1983) Kansai Society of Naval Architects, Japan, p 465
14. Kijima K, Nakiri Y (1999) Approximate expression for hydrodynamic derivatives of ship manoeuvring motion taking into account the effect of stern shape. J West Jpn Soc Nav Archit 98:67–77
15. Watanabe I, Tomita H, Tanizawa K (1992) Statistical diagrams on the wind and waves on the north Pacific Ocean (1974–1988) (in Japanese). Report of NMRI 14 (http://www.nmri.go.jp/wavedb/wavedb.html)
16. Woud HK, Stapersma D (2002) Design of propulsion and electric power generation systems. IMarEST, p 478